

# Dark photon bursts from compact binary systems and constraints

Shaoqi Hou,<sup>1,\*</sup> Shuxun Tian,<sup>2</sup> Shuo Cao,<sup>2</sup> and Zong-Hong Zhu<sup>1,2,†</sup>

<sup>1</sup>*School of Physics and Technology, Wuhan University, Wuhan, Hubei 430072, China*

<sup>2</sup>*Department of Astronomy, Beijing Normal University, Beijing 100875, China*

(Dated: October 12, 2021)

In this work, we consider the burst signal of the dark photon, the hypothetical vector boson of the  $U(1)_B$  or  $U(1)_{B-L}$  gauge group, generated by a compact binary star system. The absence of the signal in the laser interferometer puts bounds on the coupling constant  $\epsilon$  to the ordinary matter. It turns out that if the dark photon is massless,  $\epsilon^2$  is on the order of  $10^{-37} - 10^{-33}$  at most; in the massive case, the upper bound of  $\epsilon^2$  is about  $10^{-38} - 10^{-31}$  in the mass range from  $10^{-19}$  eV to  $10^{-11}$  eV. These are the first bounds derived from the interferometer observations independent of the assumption of dark photons being dark matter.

## I. INTRODUCTION

The excellent precision of the laser interferometer not only made it possible to detect gravitational waves (GWs) [1–3], but also enables the observation of new physics, such as the quantum mechanics of macroscopic objects [4, 5]. Other new physics includes new elementary particles as candidates for dark matter (DM). One of the possibilities is the dark photon (DP), which is the gauge boson associated with  $U(1)_B$  or  $U(1)_{B-L}$ , and whose mass  $m_{\gamma'}$  can be generated via the Stüeckelberg mechanism [6]. Since ordinary matters, such as the mirrors in interferometers, usually are charged under these groups, they can be accelerated by DPs. Thus, interferometers are capable of detecting DPs. In Refs. [7–10], the ultra-light DP was considered, and the stochastic background of DPs is thus coherently oscillating. Using the technique of detecting the stochastic GW background by interferometers [11, 12], DP model was highly constrained.

Here, we continue to test the DP model with GW interferometers. Instead of assuming that DPs constitute DM and using the observed DM density, we will study the emission of DPs by orbiting compact stars, just like the emission of ordinary photons by electrically charged particles that are accelerated. The generated DPs reach the interferometer, and similarly to GWs, cause strain which can be measured. Since the observed GW waveforms agree with predictions of general relativity (GR) very well, the DP model can thus be bounded.

Very interestingly, the induced strain by DPs is an explicit function of the source redshift in the frequency domain, if DP is massive. This enables the measurement of the redshift directly with DP radiation. Together with the luminosity distance determined with GWs (the idea of standard siren [13]), the measurement of DP radiation with the laser interferometer may play important roles in cosmology. Of course, the DP has not been detected. But our result may stimulate the search for suitable matter field radiation like DPs to determine the redshift.

Besides the methods presented in Refs. [7–10] and in the current work, one can also constrain DP parameters via the measurement of the violation of the equivalence principle [14, 15]. Indeed, as long as objects carry different ratios of “dark charge” to mass, they accelerate differently in the same uniform “electric” field of the DP, so the universal free-fall is violated [16]. The study of black hole superradiance might also provide strong constraints [17–22], just like the superradiance of scalar particles [23]. In the end, the charged stars under  $U(1)_B$  or  $U(1)_{B-L}$  may change their positions due to the DP radiation, so Gaia mission and the like are capable of detecting DPs [24].

Cardoso *et al.* also considered the emission of the vector boson of a hidden  $U(1)$  symmetry by binary systems [25]. The emission carries more energy of the binary system away, and modifies the phase evolution of the GW. This can be used to test the vector boson model. In the current work, the presence of DPs is inferred directly from the strain induced by them, instead of from the GW strain. The motion of the binary stars with the electric and magnetic charges is also investigated in Refs. [26, 27], where more complicated orbits exist and the attention were still on the GW waveform. Moreover, none of them considered massive vector bosons.

This work is organized as follows. Section II reviews the basics of DPs, especially the equations of motion and the energy-momentum tensor that are useful for computing DP radiation and the power carried away. Based on this, the DP radiation is computed in Sec. III. There, one first notices the changes in the central force due to new  $U(1)_B$  or  $U(1)_{B-L}$  interaction in Sec. III A. Then, one can calculate the “electric” dipole radiation following the technique learned in Ref. [28] in Sec. III B, followed by the discussion on the “magnetic” dipole and “electric” quadrupole radiation in Sec. III C. Section IV focuses on how the DP radiation induces strain in the laser interferometer, and by requiring the signal-to-noise ratio of this strain be small enough, the constraints can be obtained, as presented in Sec. V. Section VI concludes this work.

\* hou.shaoqi@whu.edu.cn

† zhuzh@whu.edu.cn

## II. THE BASICS OF DARK PHOTONS

The action of the DP  $A^\mu = (V/c, \vec{A})$  takes that of the Proca field [28],

$$\mathcal{L} = -\frac{1}{4\mu_0} F_{\mu\nu} F^{\mu\nu} + \frac{\mathbf{m}^2}{2\mu_0} A_\mu A^\mu - \epsilon e J_\mu A^\mu, \quad (1)$$

where  $F_{\mu\nu} = \partial_\mu A_\nu - \partial_\nu A_\mu$  is the field strength,  $\epsilon$  the DP coupling constant with the matter,  $e$  the electric charge,  $\mu_0$  the permeability for vacuum,  $\mathbf{m} = m_\gamma c/\hbar$  the inverse Compton wavelength, and  $J^\mu = (c\rho, \vec{j})$  the  $B$  or  $B-L$  number flux. The mostly minus sign convention for the metric is used. The equations of motion are given by

$$\nabla^\nu \nabla_\nu A_\mu + \mathbf{m}^2 A_\mu = \mu_0 \epsilon e J_\mu, \quad (2)$$

$$\nabla_\mu A^\mu = 0, \quad (3)$$

where the second equation becomes a gauge condition in the massless case. These set of equations can also be written in the following equivalent form,

$$\nabla \cdot \vec{E} + \mathbf{m}^2 V = \frac{\epsilon e \rho}{\epsilon_0}, \quad (4)$$

$$\nabla \times \vec{H} - \epsilon_0 \frac{\partial}{\partial t} \vec{E} + \frac{\mathbf{m}^2}{\mu_0} \vec{A} = \epsilon e \vec{j}, \quad (5)$$

$$\nabla \cdot \vec{H} = 0, \quad \nabla \times \vec{E} + \mu_0 \frac{\partial}{\partial t} \vec{H} = 0, \quad (6)$$

$$\nabla \cdot \vec{A} + \frac{1}{c^2} \frac{\partial}{\partial t} V = 0, \quad (7)$$

where  $\epsilon_0$  is the dielectric constant of vacuum, and  $\vec{E} = -\nabla V - \partial \vec{A}/\partial t$  and  $\vec{H} = \nabla \times \vec{A}/\mu_0$  are the ‘‘electric’’ and ‘‘magnetic’’ fields for the DP.

The test particles, such as the mirrors in the interferometer, would be accelerated if there exists nontrivial DP field with the following 3-acceleration,

$$\vec{a} = \frac{\epsilon e N}{m} (\vec{E} + \vec{v} \times \vec{B}), \quad (8)$$

with  $\vec{B} = \mu_0 \vec{H}$ . Also,  $N = \sigma m_\chi/m_p + m_\chi'/m_n$  is  $B$  (if  $\sigma = 1$ ) or  $B-L$  (if  $\sigma = 0$ ) number, where  $m_p$  and  $m_n$  are proton and neutron masses,  $\chi$  and  $\chi'$  are the mass fractions for protons and neutrons, respectively. This enables the use of the GW interferometers to detect the DP produced by the binary system.

Finally, the stress-energy tensor can be easily obtained by the variation of the action with respect to  $g^{\mu\nu}$ , given by [28]

$$T_{\mu\nu} = \frac{1}{\mu_0} \left[ F_{\mu\rho} F^\rho{}_\nu + \frac{1}{4} g_{\mu\nu} F_{\rho\sigma} F^{\rho\sigma} + \mathbf{m}^2 \left( A_\mu A_\nu - \frac{1}{2} g_{\mu\nu} A_\rho A^\rho \right) \right].$$

The temporal-spatial components are useful for computing the energy flux density, which is

$$T^{0j} = \frac{1}{c} \left( \vec{E} \times \vec{H} + \frac{\mathbf{m}^2}{\mu_0} \Phi \vec{A} \right)^j,$$

so one can recognize the Poynting vector

$$\vec{S}_m = \vec{E} \times \vec{H} + \frac{\mathbf{m}^2}{\mu_0} \Phi \vec{A},$$

where the first term is the Poynting vector in the massless case [28]. Since in our calculation, we treat all fields complex functions, the Poynting vector is

$$\vec{S}_m = \frac{1}{2} \Re \left( \vec{E} \times \vec{H}^* + \frac{\mathbf{m}^2}{\mu_0} V \vec{A}^* \right), \quad (9)$$

where  $\Re$  means to take the real part and  $\vec{H} = \vec{B}/\mu_0$ . This expression is used to calculate the radiated energy by the binary system.

Note that one assumes the flat spacetime background in writing down the above expressions. Although in the vicinity of the binary system, the spacetime is curved, the curvature is small. The perturbations to the dark photon radiation due to the curvature will be of the higher orders, so we will ignore them. With these equations, one can compute the DP radiation produced by a binary system.

## III. DARK PHOTON RADIATION FROM A BINARY SYSTEM

In the classical electrodynamics, two opposite charges orbiting around each other radiate light [28]. Similarly, two orbiting stars may also emit DPs. In this section, we will consider DP radiation up to the ‘‘electric’’ quadrupole order, just like the ordinary photon radiation.

### A. Modified central force

Since one considers a new  $U(1)$  symmetry [29], the orbital motion of binary stars would be modified becomes of the new interaction induced by the DP field strength  $(\vec{E}, \vec{B})$ . By the temporal component of Eq. (2), in the static case, the scalar potential is the Yukawa potential,

$$V = \frac{\epsilon e N}{4\pi\epsilon_0 r} e^{-\mathbf{m}r}, \quad (10)$$

due to a star with the new  $U(1)$ -charge  $eN$ . We will consider the use of interferometers to detect DPs, so  $10^{-19} \text{ eV} < m_\gamma c^2 < 10^{-11} \text{ eV}$ , corresponding to the Compton wavelength in the range of  $(10^4 \text{ m}, 10^{12} \text{ m})$ , which is much smaller than the distances between stars in a binary system at least in the inspiral stage. Therefore, one can ignore the exponential factor in describing the motion of the stars with masses  $m_1$  and  $m_2$ , that is, the acceleration of the effective one body problem is [25]

$$r\omega^2 = G \frac{M}{r^2} - \frac{\epsilon^2 e^2 N_1 N_2}{4\pi\epsilon_0 r^2} \frac{M}{m_1 m_2} = G' \frac{M}{r^2}, \quad (11)$$

Binary	$m_1(M_\odot)$	$m_2(M_\odot)$	$z$
GW150914	35.6	30.6	0.09
GW200105	8.9	1.9	0.06
GW170817	1.46	1.27	0.01
EMRI	$10^5$	10	0.2
IMRI	$10^5$	$10^3$	0.8
IMBH	$5 \times 10^3$	$4 \times 10^3$	2.0
SMBH	$5 \times 10^6$	$4 \times 10^6$	5.0

TABLE I. Source properties. The first 3 rows are taken from Refs. [33, 34]. The remaining 4 rows are suggested by Ref. [39], where EMRI stands for extreme mass-ratio inspiral, IMRI stands for intermediate mass-ratio inspiral, IMBH intermediate mass black hole binary, and SMBH supermassive black hole binary.

with  $M = m_1 + m_2$ . One can thus define an effective gravitational constant  $G' = G - \frac{\epsilon^2 e^2}{4\pi\epsilon_0} \zeta_1 \zeta_2$  with  $\zeta = N/m = \sigma\chi/m_p + \chi'/m_n$ .

Of course,  $G'$  should be very close to  $G$ , otherwise the orbital motion of binary stars would be modified so much that one can detect the difference easily, which has not happened yet [30–32]. So one can require that  $G' \approx G$  to bound  $\epsilon^2$ . In this work, we choose the binary systems in Table I to constrain  $\epsilon^2$ . The first three sources [33, 34] can emit DPs observable by the ground-based interferometers like aLIGO, Einstein Telescope (ET) [35] and Cosmic Explorer (CE) [36]. They can also be observed by the DECihertz laser Interferometer Gravitational wave Observatory (DECIGO) and its downscale version, B-DECIGO [37, 38]. The remaining four sources are for LISA, where EMRI stands for extreme mass-ratio inspiral, IMRI stands for intermediate mass-ratio inspiral, IMBH intermediate mass black hole binary, and SMBH supermassive black hole binary [39]. One also assumes that the mass fraction  $\chi$  of protons in a black hole is approximately 0.5, and  $\chi = 0$  for a neutron star. Then, one finds out that

$$\epsilon^2 \lesssim (8.1 - 32.5) \times 10^{-37} \quad (12)$$

for both gauge groups, independent of the mass  $m_{\gamma'}$ .

### B. “Electric” dipole radiation

Now, consider the DP radiation. The solution to the spatial components of Eq. (2) is generally given by

$$\begin{aligned} \vec{A}(t, \vec{x}) = & \frac{\mu_0 \epsilon e}{4\pi} \left[ \int d^3 x' \frac{\vec{j}(t - |\vec{x} - \vec{x}'|/c, \vec{x}')}{|\vec{x} - \vec{x}'|} \right. \\ & \left. - \int cd t' d^3 x' \Theta(\Delta|x|) \frac{\mathbf{m}^2 J_1(\zeta)}{\zeta} \vec{j}(t', \vec{x}') \right], \end{aligned} \quad (13)$$

where  $\zeta = \mathbf{m} \sqrt{c^2(t-t')^2 - |\vec{x} - \vec{x}'|^2}$  and  $\Delta|x| = c(t-t') - |\vec{x} - \vec{x}'|$ . Note that in the massive case, the Green

function is [40]

$$G(ct, \vec{x}) = \frac{\delta(ct - |\vec{x}|)}{|\vec{x}|} - \Theta(ct - |\vec{x}|) \frac{\mathbf{m} J_1(\mathbf{m} \sqrt{c^2 t^2 - \vec{x}^2})}{\sqrt{c^2 t^2 - \vec{x}^2}},$$

where  $J_1(z)$  is the Bessel function of the first kind. Since  $J_1(0) = 0$ , this Green function smoothly reduces to the one for the massless DP. So in the massless case,  $\vec{A}(t, \vec{x})$  is given by the first integral in Eq. (13).

In the radiation zone, one can approximate  $|\vec{x} - \vec{x}'| \approx R - \hat{n} \cdot \vec{x}'$  with  $R = |\vec{x}|$  and  $\hat{n} = \vec{x}/R$ . If one assumes the density  $\rho(t, \vec{x}) = \rho(\vec{x})e^{-i\omega t}$  and the 3-current  $\vec{j}(t, \vec{x}) = \vec{j}(\vec{x})e^{-i\omega t}$ , one obtains the following approximation [28, 41]

$$\begin{aligned} \vec{A}(\vec{x}) \approx & \frac{\mu_0 \epsilon e}{4\pi} \frac{e^{i\omega R/c}}{R} \int d^3 x' \vec{j}(\vec{x}') (1 - ik\hat{n} \cdot \vec{x}') \\ & - \frac{\mu_0 \epsilon e}{4\pi R} \int d^3 x' \int_0^\infty d\zeta J_1(\zeta) \vec{j}(\vec{x}') \times \\ & e^{i\frac{\omega}{c} R \sqrt{1 + (\zeta/\mathbf{m}R)^2}} \left[ 1 - i\frac{\omega}{c} \frac{\hat{n} \cdot \vec{x}'}{\sqrt{1 + (\zeta/\mathbf{m}R)^2}} \right]. \end{aligned}$$

Here, we have omitted a factor of  $e^{-i\omega t}$ . Once  $\vec{A}$  is determined, one knows that

$$V(\vec{x}) = -i \frac{c^2}{\omega} \nabla \cdot \vec{A}(\vec{x}), \quad (14)$$

$$\vec{H} = \frac{1}{\mu_0} \nabla \times \vec{A}, \quad (15)$$

$$\vec{E} = \frac{i}{\omega \epsilon_0} \nabla \times \vec{H} + \frac{i}{\omega} \mathbf{m}^2 c^2 \vec{A}. \quad (16)$$

The first equation is due to Eq. (7), and the last one due to Eq. (5).

Following Ref. [28], one introduces the “electric” dipole, “magnetic” dipole, and “electric” quadrupole moments,

$$\vec{D}_e = \int \vec{x} \rho(\vec{x}) d^3 x, \quad \vec{D}_m = \frac{1}{2} \int \vec{x} \times \vec{j}(\vec{x}) d^3 x, \quad (17)$$

$$Q_{jk} = \int 3x_j x_k \rho(\vec{x}) d^3 x, \quad (18)$$

respectively. Their variations lead to the emission of DPs.

Let us consider first the field strength related to the “electric” dipole moment. Assuming the binary stars move around each other in a quasi-circular orbit in the  $xOy$  plane, one can check that

$$\begin{aligned} \vec{D}_e = d_e \hat{\mathcal{E}}, \quad d_e = & \eta^{8/15} \mathcal{M} \left( \frac{G' \mathcal{M}}{\omega^2} \right)^{1/3} \xi_e, \\ \hat{\mathcal{E}} = (1, i, 0), \quad \xi_e = & \sigma \frac{\Delta\chi}{m_p} + \frac{\Delta\chi'}{m_n}, \end{aligned}$$

where  $\eta = m_1 m_2 / M^2$  is the symmetric mass ratio, and  $\mathcal{M} = \eta^{3/5} M$  is the chirp mass. In addition,  $\Delta\chi = \chi_1 - \chi_2$

with  $\chi_1$  and  $\chi_2$  the proton mass fractions of the two stars, and  $\Delta\chi' = \chi'_1 - \chi'_2$  with  $\chi_1$  and  $\chi_2$  the neutron mass fractions.

The variation of  $\vec{D}_e$  sources

$$\vec{A}_1 = -\frac{i\mu_0\epsilon\omega}{4\pi R} \left[ e^{i\omega R/c} - I_0^{(\omega)}(R) \right] \vec{D}_e, \quad (19)$$

where we have defined the symbol,

$$I_n^{(\omega)}(R) = \int_0^\infty d\zeta J_1(\zeta) \frac{e^{i\frac{\omega}{c}R\sqrt{1+(\zeta/mR)^2}}}{[1+(\zeta/mR)^2]^{n/2}}. \quad (20)$$

In the radiation zone, it is known that [41]

$$I_n^{(\omega)} \approx e^{i\omega R/c} - \left[ 1 - \left( \frac{mc}{\omega} \right)^2 \right]^{\frac{n-1}{2}} e^{i\frac{\omega R}{c} \sqrt{1 - \left( \frac{mc}{\omega} \right)^2}}, \quad (21)$$

when  $\omega > mc$ ; otherwise,  $I_n^{(\omega)} \approx e^{i\omega R/c}$ . The scalar potential is useful for calculating the radiated power, given by

$$V_1 = -\frac{i\mu_0 c \omega \epsilon \epsilon}{4\pi R} \left[ e^{i\omega R/c} - I_1^{(\omega)}(R) \right] \hat{n} \cdot \vec{D}_e. \quad (22)$$

The ‘‘magnetic’’ and ‘‘electric’’ fields are thus

$$\vec{H}_1 = \frac{\epsilon\omega^2}{4\pi c R} \left[ e^{i\omega R/c} - I_1^{(\omega)}(R) \right] \hat{n} \times \vec{D}_e, \quad (23)$$

$$\begin{aligned} \vec{E}_1 = \frac{\omega^2 \epsilon \epsilon}{4\pi \epsilon_0 c^2 R} & \left\{ \left[ e^{i\omega R/c} - I_2^{(\omega)}(R) \right] \hat{n} \times (\vec{D}_e \times \hat{n}) \right. \\ & \left. + \left( \frac{mc}{\omega} \right)^2 \left[ e^{i\omega R/c} - I_0^{(\omega)} \right] \vec{D}_e \right\}. \end{aligned} \quad (24)$$

In the above computation, one uses the relation  $\partial_j I_n^{(\omega)}(R) \approx i\frac{\omega}{c} \hat{n}_j I_{n+1}^{(\omega)}(R)$ . These can be used to calculate the Poynting vector  $\vec{S}_1$ , and then, integrate it over a 2-sphere at a large  $R$  to get the power radiated

$$\mathcal{P}_1 = \frac{\epsilon^2 e^2 \omega^4}{6\pi \epsilon_0 c^3} d_e^2 \frac{1 + (mc/\omega)^2/2}{\sqrt{1 - (mc/\omega)^2}} \Theta(\omega - mc),$$

where the average over the wavelength has been performed. The total energy of the binary system in GR is [42]

$$E = -\frac{(GM\omega)^{2/3}}{2} \mathcal{M}. \quad (25)$$

Now, in this work,  $G$  should be replaced by  $G'$ . The orbital frequency changes due to this is thus [43]

$$\dot{f}_1 = \frac{\epsilon^2 e^2 \omega^3}{4\pi^2 \epsilon_0 c^3} \eta^{2/5} \mathcal{M} \xi_e^2 \frac{1 + (mc/\omega)^2/2}{\sqrt{1 - (mc/\omega)^2}} \Theta(\omega - mc).$$

This is the leading order DP correction to the orbital frequency evolution.

### C. ‘‘Magnetic’’ dipole and ‘‘electric’’ quadrupole radiation

Similar computation can be done for the ‘‘magnetic’’ dipole and the ‘‘electric’’ quadrupole radiation. Following Ref. [28], the variations of  $\vec{D}_m$  and  $Q_{jk}$  induce the following potentials,

$$V_2 = 0, \quad \vec{A}_2 = \frac{i\mu_0 \omega \epsilon \epsilon}{4\pi c R} \left[ e^{i\omega R/c} - I_2^{(\omega)}(R) \right] \hat{n} \times \vec{D}_m,$$

$$V_3 = -\frac{\mu_0 \omega^2 \epsilon \epsilon}{6\pi R} \left[ e^{i2\omega R/c} - I_2^{(2\omega)}(R) \right] \hat{n} \cdot \vec{Q}(\hat{n}),$$

$$\vec{A}_3 = -\frac{\mu_0 \omega^2 \epsilon \epsilon}{6\pi c R} \left[ e^{i2\omega R/c} - I_1^{(2\omega)}(R) \right] \vec{Q}(\hat{n}),$$

respectively. Here, the ‘‘magnetic’’ dipole and ‘‘electric’’ quadrupole moments take the following forms,

$$\vec{D}_m = d_m \hat{\mathcal{M}}, \quad d_m = \frac{\mathcal{M} c^2}{4\omega} \left( \eta \frac{G' \mathcal{M} \omega}{c^2} \frac{\omega}{c} \right)^{2/3} \xi_m,$$

$$\xi_m = \sigma \frac{\Sigma\chi - \sqrt{1-4\eta}\Delta\chi}{m_p} + \frac{\Sigma\chi' - \sqrt{1-4\eta}\Delta\chi'}{m_n},$$

$$Q_{ijk} = \mathcal{Q} \hat{\mathcal{Q}}_{jk}, \quad \mathcal{Q} = \frac{3}{\omega} d_m.$$

In these expressions,  $\Sigma\chi = \chi_1 + \chi_2$ ,  $\Delta\chi = \chi_1 - \chi_2$ ,  $\Delta\chi' = \chi'_1 - \chi'_2$ ,  $\Sigma\chi' = \chi'_1 + \chi'_2$ ,  $\hat{\mathcal{M}} = (0, 0, 1)$ , and  $\hat{\mathcal{Q}}_{11} = -\hat{\mathcal{Q}}_{22} = -i\hat{\mathcal{Q}}_{12} = -i\hat{\mathcal{Q}}_{21} = 1$  and the remaining components vanish. Finally,  $\vec{Q}(\hat{n})$  has the following components  $Q_j(\hat{n}) = Q_{jk} \hat{n}^k$ . The corresponding ‘‘magnetic’’ and ‘‘electric’’ fields are

$$\vec{H}_2 = \frac{\omega^2 \epsilon \epsilon}{4\pi c^2 R} \left[ e^{i\omega R/c} - I_3^{(\omega)} \right] (\hat{n} \times \vec{D}_m) \times \hat{n},$$

$$\begin{aligned} \vec{E}_2 = -\frac{\omega^2 \epsilon \epsilon}{4\pi \epsilon_0 c^3 R} & \left[ e^{i\omega R/c} - I_4^{(\omega)} + \frac{m^2 c^2}{\omega^2} \times \right. \\ & \left. \left( e^{i\omega R/c} - I_2^{(\omega)} \right) \right] \hat{n} \times \vec{D}_m, \end{aligned}$$

$$\vec{H}_3 = -i \frac{\omega^3 \epsilon \epsilon}{3\pi c^2 R} \left[ e^{i2\omega R/c} - I_2^{(2\omega)} \right] \hat{n} \times \vec{Q}(\hat{n}),$$

$$\begin{aligned} \vec{E}_3 = -\frac{i\omega^3 \epsilon \epsilon}{3\pi \epsilon_0 c^3 R} & \left[ \left( e^{i2\omega R/c} - I_3^{(2\omega)} \right) \hat{n} \times [\vec{Q}(\hat{n}) \times \hat{n}] \right. \\ & \left. + \left( \frac{mc}{2\omega} \right)^2 \left( e^{i2\omega R/c} - I_1^{(2\omega)} \right) \vec{Q}(\hat{n}) \right], \end{aligned}$$

which contribute radiated powers given by

$$\mathcal{P}_2 = \frac{\omega^4 \epsilon^2 e^2}{12\pi \epsilon_0 c^5} d_m^2 \left[ 1 - \left( \frac{mc}{\omega} \right)^2 \right]^{3/2} \Theta(\omega - mc),$$

$$\mathcal{P}_3 = \frac{\omega^4 \epsilon^2 e^2}{45\pi \epsilon_0 c^5} d_m^2 \sqrt{1 - \left( \frac{mc}{2\omega} \right)^2} \left[ 1 + \frac{2}{3} \left( \frac{mc}{2\omega} \right)^2 \right] \times \Theta(2\omega - mc).$$

Therefore, the frequency evolves according to

$$\begin{aligned} \dot{f}_2 &= \frac{\epsilon^2 e^2}{128\pi^2 \epsilon_0} \left(\frac{\omega}{c}\right)^3 \mathcal{M} \left(\frac{GM\omega}{c^2} \frac{\omega}{c}\right)^{2/3} \xi_m^2 \times \\ &\quad \left[1 - \left(\frac{mc}{\omega}\right)^2\right]^{3/2} \Theta(\omega - mc), \\ \dot{f}_3 &= \frac{\epsilon^2 e^2}{480\pi^2 \epsilon_0} \left(\frac{\omega}{c}\right)^3 \mathcal{M} \left(\frac{GM\omega}{c^2} \frac{\omega}{c}\right)^{2/3} \xi_m^2 \times \\ &\quad \sqrt{1 - \left(\frac{mc}{2\omega}\right)^2} \left[1 + \frac{2}{3} \left(\frac{mc}{2\omega}\right)^2\right] \Theta(2\omega - mc), \end{aligned}$$

corresponding to  $\mathcal{P}_2$  and  $\mathcal{P}_3$ , respectively.

Then, the total change in the orbital frequency evolution due to the DP radiation is

$$\dot{f}_{\gamma'} = \dot{f}_1 + \dot{f}_2 + \dot{f}_3, \quad (26)$$

omitting higher order contributions. This would definitely affect the phase evolution of the GW emitted simultaneously [25, 44]. However, in the following discussion, one assumes  $\dot{f}_{\gamma'}$  due to the DP radiation is much smaller than that due to the GW given by,

$$\dot{f}_{\text{gw}} = \frac{48}{5\pi} \left(\frac{c^3}{G'M}\right)^2 \left(\frac{G'M\omega}{c^2} \frac{\omega}{c}\right)^{11/3}. \quad (27)$$

otherwise  $\dot{f}$  would cause large enough GW dephasing which should be observable. One can check that this assumption implies that the following upper bound is sufficient,

$$\epsilon^2 \lesssim 10^{-37}, \quad (28)$$

and later, one ignores the effect of  $\dot{f}_{\gamma'}$ . This requirement also implies that one has only to consider the effect of the DP radiation up to the order of  $\epsilon^2$ .

The total “electric” field strength is  $\vec{E} = \vec{E}_1 + \vec{E}_2 + \vec{E}_3 + \dots$  with the dots representing higher-order corrections. This field will accelerate mirrors in interferometers. The responses are to be computed below.

#### IV. INTERFEROMETER RESPONSES TO DARK PHOTONS

Let us assume the two mirrors of one arm (labeled by  $n = 1, 2$ ) of an interferometer are located at  $\vec{x}_1^{(n)}$  and  $\vec{x}_2^{(n)}$  such that  $\vec{L}^{(n)} = \vec{x}_1^{(n)} - \vec{x}_2^{(n)}$  with  $|\vec{L}^{(n)}| = L$  if there is no dark photon radiation. These mirrors move at very small speeds, so the “Lorentz force” is basically determined by the “electric field”  $\vec{E}$ . Integrating Eq. (8) twice with  $\vec{B}$  ignored, one obtains the change in the position of the mirror  $\vec{x}_1^{(n)}$ ,

$$\Delta \vec{x}_1^{(n)} = \frac{\epsilon e N}{m} \int dt \int dt' \vec{E}(\vec{x}_1^{(n)}), \quad (29)$$

and a similar expression for the mirror  $\vec{x}_2^{(n)}$ . So the total change in  $\vec{L}^{(n)}$  is

$$\begin{aligned} \Delta \vec{L}^{(n)} &= \Delta \vec{x}_1^{(n)} - \Delta \vec{x}_2^{(n)} \\ &\approx \frac{\epsilon e N}{m} \int dt \int dt' \vec{L}^{(n)} \cdot \nabla \vec{E}(\vec{x}_2^{(n)}), \end{aligned} \quad (30)$$

where the approximation can be taken becomes the wavelength of the dark photon radiation is on the same order as that of the GW, larger than  $L$ . Since the change in the arm length is  $\Delta L^{(n)} = \hat{L}^{(n)} \cdot \Delta \vec{L}^{(n)}$  with  $\hat{L}^{(n)} = \vec{L}^{(n)}/L$ , the strain induced by the dark photon radiation is thus

$$h = \frac{\Delta L^{(1)} - \Delta L^{(2)}}{L} = \frac{\epsilon e N}{m} D_{jk} \int dt \int dt' \partial^j E^k, \quad (31)$$

where  $D_{jk} = \hat{L}_j^{(1)} \hat{L}_k^{(1)} - \hat{L}_j^{(2)} \hat{L}_k^{(2)}$  is the detector configuration tensor. In the following, we set  $\chi \approx \chi' \approx 0.5$  for mirrors. One should realize that in the above derivation, one does not assume the angle between the two arms, so this result applies to ground-based interferometers. It might also be useful for space-borne detectors, such as DECIGO/B-DECIGO [37, 38, 45, 46] and LISA [47].

Now, substituting the “electric” field determined in the previous section, one finds the strain  $h(t)$  in the time domain, and furthermore, using the stationary-phase approximation [44, 48], one can determine the strain in the frequency domain, given by

$$\begin{aligned} \tilde{h}(f) &= \frac{1}{4} \sqrt{\frac{5\pi}{3}} \frac{\epsilon^2 e^2}{4\pi\epsilon_0 c^2 R} \frac{N}{m} e^{-i\Phi_1(\omega)} \left\{ \frac{\eta^{8/15}}{i} \frac{GM^2}{c^3} \right. \\ &\quad \left. \left(\frac{GM\omega}{c^2} \frac{\omega}{c}\right)^{-3/2} \xi_e \left[ \left(1 - e^{-i\omega R/c} I_3^{(\omega)}\right) F_1 \right. \right. \\ &\quad \left. \left. + \left(\frac{m_z c}{\omega}\right)^2 \left(1 - e^{-i\omega R/c} I_1^{(\omega)}\right) F_1' \right] + i \frac{\eta^{2/3}}{4} \right. \\ &\quad \left. \frac{GM^2}{c^3} \left(\frac{GM\omega}{c^2} \frac{\omega}{c}\right)^{-7/6} \xi_m \left[ 1 - e^{-i\omega R/c} I_5^{(\omega)} \right. \right. \\ &\quad \left. \left. + \left(\frac{m_z c}{\omega}\right)^2 \left(1 - e^{-i\omega R/c} I_3^{(\omega)}\right) \right] F_2 \right\}_{\omega=2\pi f} \\ &\quad + \frac{1}{4} \sqrt{\frac{5\pi}{3}} \frac{\epsilon^2 e^2}{4\pi\epsilon_0 c^2 R} \frac{N}{m} \frac{2\eta^{2/3} GM^2}{c^3} \left(\frac{GM}{c^2} \frac{\omega}{c}\right)^{-7/6} \\ &\quad \xi_m e^{-i\Phi_2(\omega)} \left[ \left(1 - e^{-i2\omega R/c} I_4^{(2\omega)}\right) \right. \\ &\quad \left. F_3 - \left(\frac{m_z c}{2\omega}\right)^2 \left(1 - e^{-i2\omega R/c} I_2^{(2\omega)}\right) F_3' \right]_{\omega=\pi f}, \end{aligned}$$

where  $f$  is the frequency in the Fourier transformation,  $F_1 = D^{jk} \hat{n}_j [\hat{n} \times (\hat{e} \times \hat{n})]_k$ ,  $F_1' = D^{jk} \hat{n}_j \hat{e}_k$ ,  $F_2 = D^{jk} \hat{n}_j [\hat{n} \times \hat{\mathcal{M}}]_k$ ,  $F_3 = D^{jk} \hat{n}_j \{\hat{n} \times [\hat{n} \times \hat{\mathcal{Q}}(\hat{n})]\}_k$ , and  $F_3' = D^{jk} \hat{n}_j \hat{\mathcal{Q}}_k(\hat{n})$ .  $R$  has to be replaced by the luminosity distance  $d_L$ , and all the quantities on the right-hand side should be understood as the measured ones in the detector frame. In particular,  $\mathbf{m}_z = \mathbf{m}(1+z)$  is the redshifted DP mass with  $z$  the redshift of the source. In

addition,  $\tilde{\Phi}_1(\omega) = \omega t_c - \Phi_c - \frac{\pi}{4} + \frac{3}{256} \left(\frac{GM\omega}{c^3}\right)^{-5/3}$ , and  $\tilde{\Phi}_2(\omega) = 2\tilde{\Phi}_1(\omega) + \frac{\pi}{4}$  with  $t_c$  and  $\Phi_c$  the fiducial coalescence time and (orbital) phase, respectively.

The signal-to-noise ratio  $\rho$  can be calculated from [49]

$$\rho^2 = 4 \int \frac{\langle |\tilde{h}(f)|^2 \rangle}{S_n(f)} df, \quad (32)$$

where  $\langle \rangle$  means to take the angular average, as the angular resolution of a single laser interferometer is still poor. By requiring  $\rho < 8$ , one can determine the bounds on  $\epsilon^2$  and  $m_{\gamma'}$ , since no dark photon radiation has been observed yet.

Before presenting the constraints, one should note the presence of  $\mathbf{m}_z$  in the above waveform. If DPs exist and  $\mathbf{m}$  can be measured independently and locally, the above waveform explicitly depends on the source redshift  $z$ . Thus,  $z$  can be determined directly from the DP induced waveform, and this has a great significance in cosmology, especially resolving the Hubble tension [50, 51].

## V. CONSTRAINTS

We will determine the constraints from the absence of DP signals in some of the observed GW events by aLIGO, and by assuming other interferometers (e.g., ET, CE, DECIGO, B-DECIGO and LISA, et. al.) cannot detect DPs either. To compute SNR, one needs to set the integration limits in Eq. (32). We will set the lower limit  $f_{\text{lower}}$  to be 1 Hz for ET, 5 Hz for aLIGO and CE,  $10^{-3}$  Hz for DECIGO and B-DECIGO, and  $10^{-4}$  Hz for LISA. The upper limit will be  $f_{\text{upper}} = \min\{f_{\text{isco}}, f_{\text{max}}\}$ , where  $f_{\text{isco}}$  is the frequency corresponding to the innermost stable circular orbit [52],

$$f_{\text{isco}} = 4.40(1 + 1.25\eta + 1.08\eta^2) \left[ \frac{M_\odot}{(1+z)(m_1 + m_2)} \right] \text{kHz},$$

and  $f_{\text{max}}$  is the upper bound of the detector sensitivity band. For ground-based interferometers,  $f_{\text{max}} = 10^4$  Hz; for DECIGO and B-DECIGO,  $f_{\text{max}} = 100$  Hz, and  $f_{\text{max}} = 1$  Hz, if LISA is used.

Figure 1 displays the characteristic strains induced by the DP radiation generated by GW150914, assuming  $\epsilon^2$  takes the upper bound set by Eq. (28). The black curves are the sensitivity curves for aLIGO (solid), ET (dot-dashed) and CE (dotted), and the remaining curves are the DP signals with the solid curves for the massless case, and the dot-dashed ones for the massive case. Since for the massive case, the radiation would be shut down if the frequency is too low, the dot-dashed curves start from  $f = 25$  Hz, which corresponds to  $m_{\gamma'} c^2 \approx 10^{-13}$  eV.

If the DP is massless, the upper bounds on  $\epsilon^2$  are listed in Table II. Numbers enclosed by brackets are for  $U(1)_{B-L}$ , and these not enclosed are for  $U(1)_B$ . From this table, one knows that aLIGO and LISA are incapable of putting stronger constraints than Eq. (28).

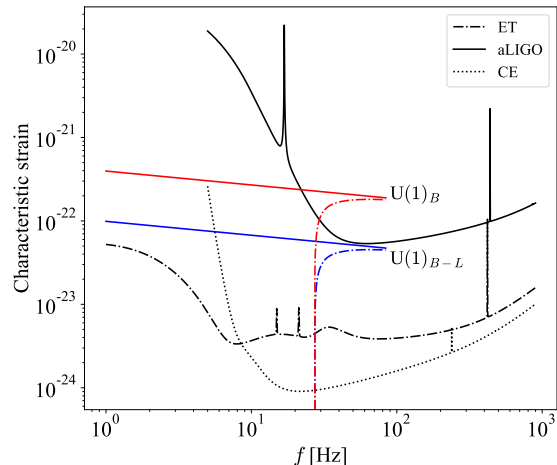


FIG. 1. The characteristic strains induced by the DP radiation generated by a GW150914-like binary system. The black solid, dot-dashed and the dotted curves are the sensitivities for aLIGO, ET and CE, respectively. The red and blue curve are signals of DP radiation for  $U(1)_B$  and  $U(1)_{B-L}$ , respectively, with the solid ones for  $m_{\gamma'} = 0$  and the dot-dashed ones for  $m_{\gamma'} \neq 0$ . Here, one chooses  $m_{\gamma'} c^2 \approx 10^{-13}$  eV for the purpose of demonstration. This mass corresponds to the Compton frequency 25 Hz. Drew with PyCBC [53].

Detector	GW150914	GW170817	GW200105	
aLIGO	1.9(7.6)	2.2(4.4)	6.8(13.3)	
ET-D	0.08(0.32)	0.11(0.23)	0.34(0.58)	
CE	0.02(0.09)	0.03(0.07)	0.10(0.18)	
DECIGO	0.02(0.07)	0.03(0.05)	0.08(0.05)	
B-DECIGO	0.21(0.86)	0.34(0.68)	1.0(0.78)	
	EMRI	IMRI	IMBH	SMBH
LISA	19.2(76.8)	1.5(6.1)	1.55(6.2)	7.5(30.0)

TABLE II. The upper bounds (in units of  $10^{-37}$ ) on  $\epsilon^2$  assuming  $m_{\gamma'} = 0$ .

If  $m_{\gamma'} \neq 0$ , the constraints are shown in Fig. 2. The upper panel displays the constraints for  $U(1)_{B-L}$ , and the lower panel is for  $U(1)_B$ . The shaded areas corresponding to the bound Eq. (28). The constraints derived from the future observations by LISA are represented by the cyan curves, as clearly labeled. The remaining curves are constraints for other detectors, as indicated by different colors. Among them, the solid curves are from GW150914, the dashed ones from GW200105, and the dot-dashed ones from GW170817. All the constraints on  $\epsilon^2$  in the lower panel are less than those in the upper panel. This figure also shows that CE and ET impose stronger constraints on  $\epsilon^2$ , while the remaining detectors mainly provide even less stringent bounds than Eq. (28).

## VI. CONCLUSION

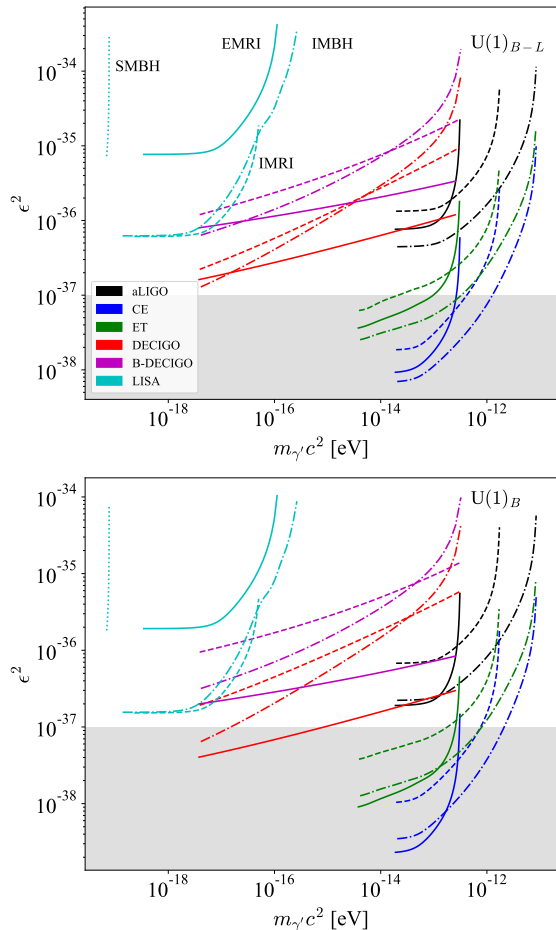


FIG. 2. Constraints on  $m_{\gamma'}$  and  $\epsilon^2$  derived from the absence of the DP signals in several interferometers. The upper panel shows the constraints for  $U(1)_{B-L}$  and upper for  $U(1)_B$ . The shaded areas are due to Eq. (28). The constraints derived from the future observations by LISA are represented by the cyan curves, as clearly labeled. The remaining curves are for other detectors. Among them, the solid curves are from GW150914, the dashed ones from GW200105, and the dot-dashed ones from GW170817. Drew with PyCBC [53] and LISA sensitivity calculator [54].

In this work, the (massive) DP radiation emitted by orbiting binary stars is computed for the first time. Its waveform up to the “electric” quadrupole radiation is obtained, which depends on the source redshift explicitly. Then, the response of the interferometer to the DP radiation is determined, valid for all possible configurations of the two arms. Since no obvious deviations from GR’s prediction have been detected in the GW strain by LIGO/Virgo, three types of constraints can be applied to the DP model: 1) the effective gravitational constant  $G' \approx G$ ; 2) the orbit of the binary system decays approximately due to the GW emission; 3) the SNR for the DP signal should be small. These requirements lead to constraints collected in Table II for massless DPs and Fig. 2 for massive DPs. Although these constraints are weaker than those reported in Refs. [7–10], they are the first constraints derived from the DP radiation without the assumption of DP being DM. Of course, in the current work, we have considered the DP radiation only in the inspiral stage of the coalescence of the binary system. Since the SNR for the GW mainly comes from the GW signal produced during the merger and ring-down stages, then if one also studies the DP radiation during these stages, one should obtain stronger constraints.

The method presented in this work is actually applicable to many other elementary particles in new physics, including other DM candidates, such as axion [55–58]. As long as these particles interact with the visible matter, they can be produced in processes such as the inspiral of binary systems, the spinning of neutron stars with mountains [59, 60], and the phase transitions in the very early universe [61]. Once they reach the interferometer, they induce new strains in addition to that due to the GW. Therefore, the GW laser interferometer also serves as a tool to detect new physics.

## ACKNOWLEDGMENTS

This work was supported by the National Natural Science Foundation of China under Grants No. 11633001, No. 11673008, No. 11922303, and No. 11920101003 and the Strategic Priority Research Program of the Chinese Academy of Sciences, Grant No. XDB23000000. ST was supported by the Initiative Postdocs Supporting Program under Grant No. BX20200065.

- [1] B. P. Abbott *et al.*, Observation of gravitational waves from a binary black hole merger, *Phys. Rev. Lett.* **116**, 061102 (2016).  
 [2] B. P. Abbott *et al.*, GW170817: Observation of gravitational waves from a binary neutron star inspiral, *Phys.*

- Rev. Lett.* **119**, 161101 (2017).  
 [3] R. Abbott *et al.*, Observation of gravitational waves from two neutron star–black hole coalescences, *Astrophys. J. Lett.* **915**, L5 (2021).  
 [4] H. Yu *et al.*, Quantum correlations between light and the

- kilogram-mass mirrors of LIGO, *Nature* **583**, 43 (2020).
- [5] C. Whittle *et al.*, Approaching the motional ground state of a 10-kg object, *Science* **372**, 1333 (2021).
- [6] H. Ruegg and M. Ruiz-Altaba, The Stueckelberg field, *Int. J. Mod. Phys. A* **19**, 3265 (2004), [arXiv:hep-th/0304245](#).
- [7] A. Pierce, K. Riles, and Y. Zhao, Searching for dark photon dark matter with gravitational-wave detectors, *Phys. Rev. Lett.* **121**, 061102 (2018).
- [8] H.-K. Guo, K. Riles, F.-W. Yang, and Y. Zhao, Searching for dark photon dark matter in LIGO O1 data, *Commun. Phys.* **2**, 155 (2019).
- [9] S. Morisaki, T. Fujita, Y. Michimura, H. Nakatsuka, and I. Obata, Improved sensitivity of interferometric gravitational-wave detectors to ultralight vector dark matter from the finite light-traveling time, *Phys. Rev. D* **103**, L051702 (2021).
- [10] R. Abbott *et al.*, Constraints on dark photon dark matter using data from LIGO’s and Virgo’s third observing run, [arXiv \(2021\)](#), [arXiv:2105.13085 \[astro-ph.CO\]](#).
- [11] T. Callister, A. S. Biscoveanu, N. Christensen, M. Isi, A. Matas, O. Minazzoli, T. Regimbau, M. Sakellariadou, J. Tasson, and E. Thrane, Polarization-based Tests of Gravity with the Stochastic Gravitational-Wave Background, *Phys. Rev. X* **7**, 041058 (2017), [arXiv:1704.08373 \[gr-qc\]](#).
- [12] B. P. Abbott *et al.* (LIGO Scientific, Virgo), Search for Tensor, Vector, and Scalar Polarizations in the Stochastic Gravitational-Wave Background, *Phys. Rev. Lett.* **120**, 201102 (2018), [arXiv:1802.10194 \[gr-qc\]](#).
- [13] B. F. Schutz, Determining the Hubble Constant from Gravitational Wave Observations, *Nature* **323**, 310 (1986).
- [14] J. Bergé, P. Brax, G. Métris, M. Pernot-Borràs, P. Touboul, and J.-P. Uzan, MICROSCOPE Mission: First Constraints on the Violation of the Weak Equivalence Principle by a Light Scalar Dilaton, *Phys. Rev. Lett.* **120**, 141101 (2018), [arXiv:1712.00483 \[gr-qc\]](#).
- [15] S. Schlamminger, K. Y. Choi, T. A. Wagner, J. H. Gundlach, and E. G. Adelberger, Test of the equivalence principle using a rotating torsion balance, *Phys. Rev. Lett.* **100**, 041101 (2008), [arXiv:0712.0607 \[gr-qc\]](#).
- [16] C. M. Will, *Theory and experiment in gravitational physics* (Cambridge, UK: Univ. Pr. (1993) 380 p, 1993).
- [17] A. Arvanitaki, M. Baryakhtar, and X. Huang, Discovering the QCD Axion with Black Holes and Gravitational Waves, *Phys. Rev. D* **91**, 084011 (2015), [arXiv:1411.2263 \[hep-ph\]](#).
- [18] M. Baryakhtar, R. Lasenby, and M. Teo, Black Hole Superradiance Signatures of Ultralight Vectors, *Phys. Rev. D* **96**, 035019 (2017), [arXiv:1704.05081 \[hep-ph\]](#).
- [19] W. E. East and F. Pretorius, Superradiant Instability and Backreaction of Massive Vector Fields around Kerr Black Holes, *Phys. Rev. Lett.* **119**, 041101 (2017), [arXiv:1704.04791 \[gr-qc\]](#).
- [20] W. E. East, Superradiant instability of massive vector fields around spinning black holes in the relativistic regime, *Phys. Rev. D* **96**, 024004 (2017), [arXiv:1705.01544 \[gr-qc\]](#).
- [21] V. Cardoso, O. J. C. Dias, G. S. Hartnett, M. Middleton, P. Pani, and J. E. Santos, Constraining the mass of dark photons and axion-like particles through black-hole superradiance, *JCAP* **03**, 043, [arXiv:1801.01420 \[gr-qc\]](#).
- [22] A. Caputo, S. J. Witte, D. Blas, and P. Pani, Electromagnetic signatures of dark photon superradiance, *Phys. Rev. D* **104**, 043006 (2021), [arXiv:2102.11280 \[hep-ph\]](#).
- [23] R. Brito, V. Cardoso, and P. Pani, Superradiance: New Frontiers in Black Hole Physics, *Lect. Notes Phys.* **906**, pp.1 (2015), [arXiv:1501.06570 \[gr-qc\]](#).
- [24] H.-K. Guo, Y. Ma, J. Shu, X. Xue, Q. Yuan, and Y. Zhao, Detecting dark photon dark matter with Gaia-like astrometry observations, *JCAP* **05**, 015, [arXiv:1902.05962 \[hep-ph\]](#).
- [25] V. Cardoso, C. F. B. Macedo, P. Pani, and V. Ferrari, Black holes and gravitational waves in models of minicharged dark matter, *JCAP* **05**, 054, [Erratum: *JCAP* 04, E01 (2020)], [arXiv:1604.07845 \[hep-ph\]](#).
- [26] L. Liu, O. Christiansen, Z.-K. Guo, R.-G. Cai, and S. P. Kim, Gravitational and electromagnetic radiation from binary black holes with electric and magnetic charges: Circular orbits on a cone, *Phys. Rev. D* **102**, 103520 (2020), [arXiv:2008.02326 \[gr-qc\]](#).
- [27] L. Liu, O. Christiansen, Z.-K. Guo, R.-G. Cai, and S. P. Kim, Gravitational and electromagnetic radiation from binary black holes with electric and magnetic charges: Elliptical orbits on a cone, [arXiv \(2020\)](#), [arXiv:2011.13586 \[gr-qc\]](#).
- [28] J. D. Jackson, *Classical Electrodynamics* (Wiley, 1998).
- [29] Either  $U(1)_B$  or  $U(1)_{B-L}$ .
- [30] R. A. Hulse and J. H. Taylor, Discovery of a pulsar in a binary system, *Astrophys. J. Lett.* **195**, L51 (1975).
- [31] B. P. Abbott *et al.* (LIGO Scientific, Virgo), Tests of General Relativity with GW170817, *Phys. Rev. Lett.* **123**, 011102 (2019), [arXiv:1811.00364 \[gr-qc\]](#).
- [32] B. P. Abbott *et al.* (LIGO Scientific, Virgo), Tests of General Relativity with the Binary Black Hole Signals from the LIGO-Virgo Catalog GWTC-1, *Phys. Rev. D* **100**, 104036 (2019), [arXiv:1903.04467 \[gr-qc\]](#).
- [33] B. P. Abbott *et al.* (Virgo and LIGO Scientific Collaborations), GWTC-1: A Gravitational-Wave Transient Catalog of Compact Binary Mergers Observed by LIGO and Virgo during the First and Second Observing Runs, *Phys. Rev. X* **9**, 031040 (2019), [arXiv:1811.12907 \[astro-ph.HE\]](#).
- [34] R. Abbott *et al.* (LIGO Scientific, KAGRA, VIRGO), Observation of Gravitational Waves from Two Neutron Star–Black Hole Coalescences, *Astrophys. J. Lett.* **915**, L5 (2021), [arXiv:2106.15163 \[astro-ph.HE\]](#).
- [35] M. Punturo *et al.*, The third generation of gravitational wave observatories and their science reach, *Gravitational waves. Proceedings, 8th Edoardo Amaldi Conference, Amaldi 8, New York, USA, June 22-26, 2009*, *Class. Quant. Grav.* **27**, 084007 (2010).
- [36] B. P. Abbott *et al.* (LIGO Scientific), Exploring the Sensitivity of Next Generation Gravitational Wave Detectors, *Class. Quant. Grav.* **34**, 044001 (2017), [arXiv:1607.08697 \[astro-ph.IM\]](#).
- [37] N. Seto, S. Kawamura, and T. Nakamura, Possibility of direct measurement of the acceleration of the universe using 0.1-Hz band laser interferometer gravitational wave antenna in space, *Phys. Rev. Lett.* **87**, 221103 (2001), [arXiv:astro-ph/0108011 \[astro-ph\]](#).
- [38] S. Isoyama, H. Nakano, and T. Nakamura, Multiband Gravitational-Wave Astronomy: Observing binary inspirals with a decihertz detector, B-DECIGO, *PTEP* **2018**, 073E01 (2018), [arXiv:1802.06977 \[gr-qc\]](#).
- [39] K. Chamberlain and N. Yunes, Theoretical Physics Implications of Gravitational Wave Observation with

- Future Detectors, *Phys. Rev. D* **96**, 084039 (2017), [arXiv:1704.08268 \[gr-qc\]](#).
- [40] E. Poisson, A. Pound, and I. Vega, The Motion of point particles in curved spacetime, *Living Rev. Rel.* **14**, 7 (2011), [arXiv:1102.0529 \[gr-qc\]](#).
- [41] J. Alsing, E. Berti, C. M. Will, and H. Zaglauer, Gravitational radiation from compact binary systems in the massive Brans-Dicke theory of gravity, *Phys. Rev. D* **85**, 064041 (2012), [arXiv:1112.4903 \[gr-qc\]](#).
- [42] M. Maggiore, *Gravitational Waves. Vol. 1: Theory and Experiments*, Oxford Master Series in Physics (Oxford University Press, Oxford, 2007).
- [43] S. Hou and Y. Gong, Constraints on Horndeski Theory Using the Observations of Nordtvedt Effect, Shapiro Time Delay and Binary Pulsars, *Eur. Phys. J. C* **78**, 247 (2018), [arXiv:1711.05034 \[gr-qc\]](#).
- [44] S. Hou, X.-L. Fan, and Z.-H. Zhu, Corrections to the gravitational wave phasing, *Phys. Rev. D* **101**, 084052 (2020), [arXiv:1911.04182 \[gr-qc\]](#).
- [45] K. Yagi and N. Seto, Detector configuration of DECIGO/BBO and identification of cosmological neutron-star binaries, *Phys. Rev. D* **83**, 044011 (2011), [Erratum: *Phys.Rev.D* 95, 109901 (2017)], [arXiv:1101.3940 \[astro-ph.CO\]](#).
- [46] T. Nakamura *et al.*, Pre-DECIGO can get the smoking gun to decide the astrophysical or cosmological origin of GW150914-like binary black holes, *PTEP* **2016**, 093E01 (2016), [arXiv:1607.00897 \[astro-ph.HE\]](#).
- [47] P. A. Seoane *et al.* (eLISA), The Gravitational Universe, arXiv e-prints (2013), [arXiv:1305.5720 \[astro-ph.CO\]](#).
- [48] S. Droz, D. J. Knapp, E. Poisson, and B. J. Owen, Gravitational waves from inspiraling compact binaries: Validity of the stationary phase approximation to the Fourier transform, *Phys. Rev. D* **59**, 124016 (1999), [arXiv:gr-qc/9901076 \[gr-qc\]](#).
- [49] N. Yunes and X. Siemens, Gravitational-Wave Tests of General Relativity with Ground-Based Detectors and Pulsar Timing-Arrays, *Living Rev. Rel.* **16**, 9 (2013), [arXiv:1304.3473 \[gr-qc\]](#).
- [50] A. G. Riess, S. Casertano, W. Yuan, L. M. Macri, and D. Scolnic, Large Magellanic Cloud Cepheid Standards Provide a 1% Foundation for the Determination of the Hubble Constant and Stronger Evidence for Physics beyond  $\Lambda$ CDM, *Astrophys. J.* **876**, 85 (2019), [arXiv:1903.07603 \[astro-ph.CO\]](#).
- [51] N. Aghanim *et al.* (Planck), Planck 2018 results. VI. Cosmological parameters, *Astron. Astrophys.* **641**, A6 (2020), [arXiv:1807.06209 \[astro-ph.CO\]](#).
- [52] C. Bonvin, C. Caprini, R. Sturani, and N. Tamanini, Effect of matter structure on the gravitational waveform, *Phys. Rev. D* **95**, 044029 (2017), [arXiv:1609.08093 \[astro-ph.CO\]](#).
- [53] A. Nitz *et al.*, [gwastro/pycbc: Pycbc release 1.18.1 \(2021\)](#).
- [54] N. Cornish, [eXtremeGravityInstitute/LISA Sensitivity: Version 1 \(2019\)](#).
- [55] R. D. Peccei and H. R. Quinn, Constraints Imposed by CP Conservation in the Presence of Instantons, *Phys. Rev. D* **16**, 1791 (1977).
- [56] J. E. Kim, Weak Interaction Singlet and Strong CP Invariance, *Phys. Rev. Lett.* **43**, 103 (1979).
- [57] M. A. Shifman, A. I. Vainshtein, and V. I. Zakharov, Can Confinement Ensure Natural CP Invariance of Strong Interactions?, *Nucl. Phys. B* **166**, 493 (1980).
- [58] M. Dine, W. Fischler, and M. Srednicki, A Simple Solution to the Strong CP Problem with a Harmless Axion, *Phys. Lett. B* **104**, 199 (1981).
- [59] G. Ushomirsky, C. Cutler, and L. Bildsten, Deformations of accreting neutron star crusts and gravitational wave emission, *Mon. Not. Roy. Astron. Soc.* **319**, 902 (2000), [arXiv:astro-ph/0001136](#).
- [60] C. J. Horowitz and K. Kadau, The Breaking Strain of Neutron Star Crust and Gravitational Waves, *Phys. Rev. Lett.* **102**, 191102 (2009), [arXiv:0904.1986 \[astro-ph.SR\]](#).
- [61] T. Hasegawa, N. Okada, and O. Seto, Gravitational waves from the minimal gauged  $U(1)_{B-L}$  model, *Phys. Rev. D* **99**, 095039 (2019), [arXiv:1904.03020 \[hep-ph\]](#).